Coding of Non-Linear White-Light Luminescence from Gold-Silicon Structures for Physically Unclonable Security Labels

Ekaterina Yu Ponkratova, Eduard I Ageev, Peter V Trifonov, Pavel I Kustov, Martin Sandomirskii, Mikhail V Zhukov, Artem I Larin, Ivan S Mukhin, Thierry Belmonte, Alexandre Nominé„ et al.

Coding of non-linear white light luminescence from gold-silicon structures for physically unclonable security labels

*Ekaterina Ponkratova Eduard Ageev Peter Trifonov Pavel Kustov Mikhail Zhukov Artem Larin Ivan Mukhin Thierry Belmonte Alexandre Nominé Stéphanie Bruyère Dmitry Zuev**

E. Yu. Ponkratova, E. I. Ageev, P. V. Trifonov, P.I. Kustov, M. V. Zhukov, A. I. Larin, I. S. Mukhin, A. Nominé, Dr. D. A. Zuev
Department of Physics and Engineering
ITMO University
Lomonosova str. 9, St. Petersburg 191002, Russia
Email Address: d.zuev@metalab.ifmo.ru
M. V. Zhukov
Laboratory of scanning probe microscopy and spectroscopy
Institute for Analytical Instrumentation RAS
St.Petersburg 198095, Russia
I. S. Mukhin
St. Petersburg Academic University
Khlopina str. 8, St. Petersburg 194021, Russia
T. Belmonte, A. Nominé, S. Bruyère
Institut Jean Lamour – CNRS – Université de Lorraine, Nancy, France

Keywords: *Security label, PUF label, nonlinear response, white light, SHG, metal-dielectric structures*

Luminescent security labels are effective platform for protection of consumer goods from counterfeiting. Despite this the lifetime of such security technology is limited due to narrow-band photoluminescent features of the label elements. In this paper, we propose a novel concept for the application of non-linear white light luminescence achieved in hybrid metal-semiconductor structures fabricated by the direct fs-laser writing for the creation of physically unclonable security labels. We demonstrate a close connection between internal composition of fabricated hybrid structures controlled on the fabrication stage and their non-linear optical signals. We show that application of decorrelation procedure based on discrete cosine transform as well as polar codes for the label coding can overcome the problem of the white-light photoluminescent spectra correlation. The applied fabrication approach and coding strategy are applied for physically unclonable label creation with high degree of device uniqueness (up to 99%) and bit uniformity (close to 0.5). Demonstrated results remove the barriers for the application of white light luminescent nanoobjects for physically unclonable label creation.

1 Introduction

Fake consumer goods cause huge financial losses in industry, affect many areas of life and also threaten to individuals, corporations and society as a whole. A striking example is counterfeiting of medicine. According to the World Health Organization, over 10% medicines in low and middle-income countries are falsified [1]. Extreme danger of counterfeit medicines is that substandard and falsified medicines can even cause lethal cases. Such data clearly illustrate that counterfeit represents one of the serious threats to humanity. Over the centuries the immense experience in protective technologies is gained and utilized for development of different designes of security labels. The safety of these methods mainly depends on technical barriers. But a wide access to the modern equipment in the global market for forgers decreases the lifetime of protective technologies applied in security labels fabrication. Therefore, the development of the novel approaches for the next-generation anti-counterfeiting systems represents a challenge for science and industry.
Among the wide set of technologies which are being elaborated for the security labels creation the luminescent nanosystems attract especial interests [2, 3]. Currently, anti-counterfeiting systems based on up and downconversion luminescent materials are widely studied and even integrated in some industrial applications, e.g. in banknotes [4]. But with time, simple luminescence-based security technologies are inevitably repeated and cannot meet protective criteria. The next steps in the luminescent security label evolution are application of new luminescent materials with high level of luminescence stability and

intensity, development of non-standard designs of luminescent security labels, etc. The common demand to all developed new types of luminescent label is that it should combine not only high security level but also low preparation cost and fabrication method simplicity [5].
From this point of view laser-assisted techniques of fabrication are very attractive. Indeed, precise control of the laser beam parameters and irradiation mode of the sample surface provide ample opportunity for realization of different designes of security labels. For example, lasers have already proven their effectiveness for the fabrication of anti-counterfeiting based on colored protection patterns on a metal surface [6, 7]. Currently the next step in the development of laser-assisted approaches for the security labels creation is fabrication of narrow-band luminescent patterns [8, 9, 10]. Such patterns are based on the narrow-band photoluminescence or combination of different luminescent systems, which, however, is a conventional approach to luminescent security label designs [3, 5]. The narrow luminescent range is an effective tool in terms of registration and decoding but such feature can be used for the label hacking and duplication. Therefore, another approaches to the luminescent labels design can be considered as availability to tune luminescent spectra under the external stimuli [11], lifetime encoding [12], application of broadband photoluminescence [13], etc. The last one can be considered as a promising approach for creation of luminescent security labels based on nanoobjects with white light photoluminescence.
In this case application of wide photo-luminescent spectral range for the label encoding/authentication eliminates problems related with reduced security lifetime of security technologies based on narrow-band photoluminescence. But from another side such feature adds difficulties related with similarity and correlation of white-light luminescent spectra utilized in coding/authentication procedures. Therefore such labels and methods for their fabrication are not still widely used.
In this paper, we demonstrate an application of single-step laser fabrication method for creation of three types of structures with different non-linear response after irradiation of the Au/Si thin film surface. To understand the origin of the non-linear response behavior the internal microstructure of the fabricated systems is studied by the HRTEM technique. The opportunity of utilization of the difference in the nonlinenar behavior as well as white-light luminescent signal of the fabricated system for creation of multilevel security labels is demonstrated.

2 Results and Discussion

2.1 Fabrication and characterization

The distinctive feature of laser-assisted nanofabrication is that one can obtain absolutely different geometries of objects created from the same sample by reconfiguration of laser-irradiation parameters. In this work, we fabricated hybrid metal-dielectric structures with different geometry features. As an initial sample, we used bi-layered Au/Si film with thicknesses 30 and 90 nm respectively on a glass substrate. The creation of structures was performed by the irradiation of the film surface in the transmittance geometry (Fig. 1a).
The fs-laser pulses with a wavelength of 1047 nm were tightly focused on the film surface in the spot with diameter D $\approx$ 4 μm. The structures were produced by moving of sample in two perpendicular directions lying in the sample surface plane and variation of incident power density (I) and of laser pulses incident at one point (N). Figure 1b illustrates SEM images of produced structures which were tilted at the angle 45 degrees relative to the normal. From this figure it can be observed, that different combinations of variable parameters lead to the formation of structures with different shapes and sizes. For instance, irradiation of the sample with a power density of 39 kW/cm^2 leads to the formation of parabolic shape structures which diameters growth with an increase of amount of incident pulses. Irradiation of the sample with a power density of 78 kW/cm^2 leads to the formation of conical shape structures with the same dependence of their diameters on N as in the previous case. Similar structures were created under irradiation with I = 117 and 156 kW/cm^2 at single and double-pulsed regimes but peaks in the center of produced structures in these regimes are more pronounced. Holes with different diameters (1-2 μm) instead of sharp peaks were noticed under irradiation with power densities of 117 and 156 kW/cm^2

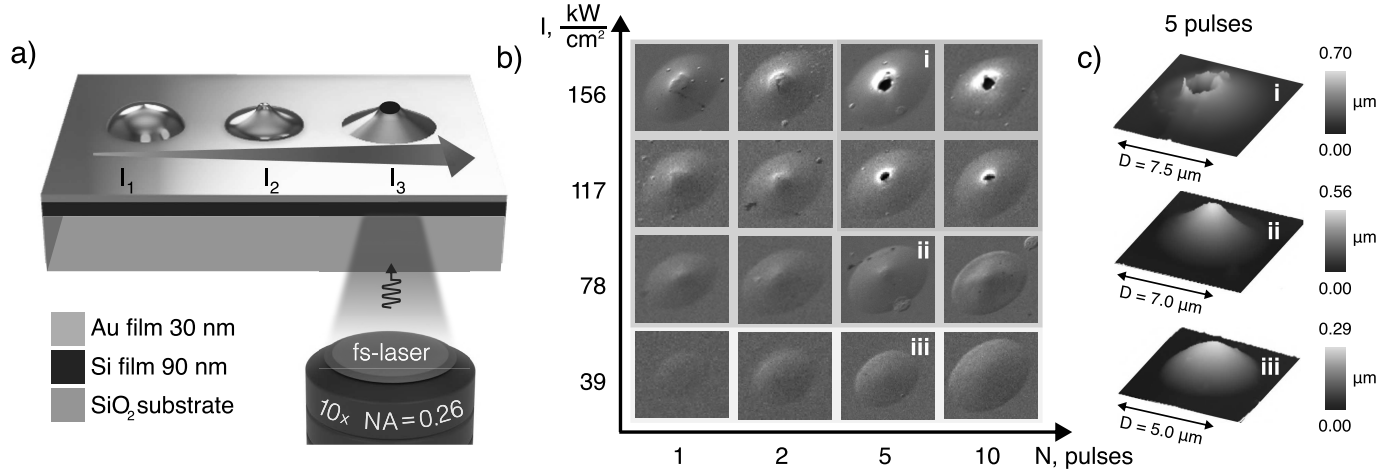

Figure 1: Hybrid metal-semiconsuctor structures. a) Fabrication scheme; b) SEM images of the hybrid structures (observation angle is 45 degrees); c) AFM images of the three typical geometries.

at 5 and 10-pulsed regimes. The proposed approach demonstrates high repeatability for the gold-silicon structures fabrication and makes possible to write arrays consisted on the nanostructures of the same type (see, Supporting information, Section 1).

To provide a detailed analysis of obtained hybrid systems with atomic resolution, Transmission electron microscopy (TEM) was applied. To see the elemental distribution inside the considered structure the Energy-Dispersive X-ray spectroscopy (EDS) mapping was also provided in the scanning mode (STEM) in parallel with the TEM analysis. Fig. 2a shows the EDS analysis of parabolic, conical and hollow shape structures.

It can be noticed from the figure that for all structures both gold (green color) and silicon (red color) films are elongated perpendicular to the surface. It is also seen that due to low plasticity, the silicon film has a sharp bending while the plastic gold film has a smooth bending profile. In addition to this, a lack of silicon film in the central part of the structure can be observed from the EDS maps. This lack of material can be explained by its possible loss during the sample preparation for the TEM measurements.

To have a more detailed analysis of the hybrid systems some parts of the map for the conical structure are chosen (marked by colorful boxes in the figure 2). The magnified boxes are also illustrated in figure 2b and they were chosen for further investigations under TEM microscopy. Figures 2c and 2b shows the corresponding TEM and High-Resolution TEM (HRTEM) images for the same areas. Fast Fourier Transform (FFT) of HRTEM areas are represented in figure 2e. From FFT HRTEM analysis, it is seen that on the edges of the structure the silicon is in the amorphous phase. Closer to central part the film consists of differently oriented grains of Si (cubic structure Fd-3m). These observations are confirmed by Fast Fourier Transform (FFT) of HRTEM areas, which results are represented in the figure 2e. It is well known that crystalline materials consist of an ordered arrangement of atoms, and incident electrons on these atoms can be diffracted only at specific angles. Diffracted at these directions electrons are seen as the spots on the image. In turn, the gold film (in green on the EDS maps) is completely crystallized on the whole FIB lamella (i.e. in the laser-irradiated zone). It should be noted that similar behavior for gold and silicon films is observed for parabolic and hollow structures, therefore the analysis for them is not represented.

These studies shade the light on the processes leading to the hybrid systems formation from the two-layered gold-silicon thin films. The shape of hybrid nanosystem is mainly determined by the modification of the gold layer. The changes in the Au film profile can be described by Marangoni effect (elasto-plastic flows model) [14, 15]. According to this model, incident pulse with the Gaussian energy distribution profile irradiates the film surface and after several picoseconds of electron-ion temperature relaxation, the gold film is heated with radial temperature gradients oriented from the center to the edges of the irradiated area. These temperature gradients lead to thermal stresses in the film which in turn in-

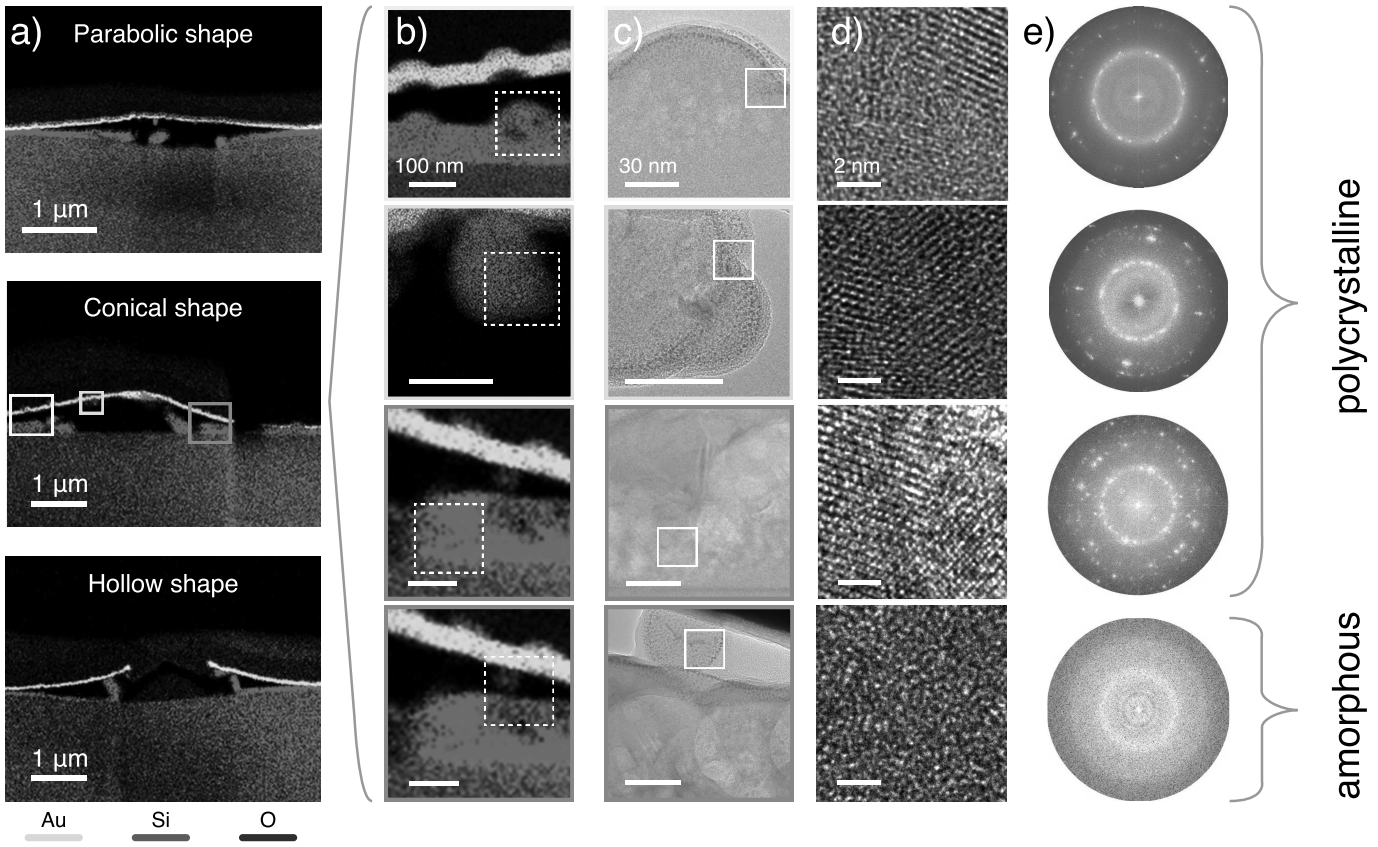

Figure 2: Analysis of the geometry and inner composition of the hybrid systems. a) STEM-EDS maps of structures cross sections which show films bending under laser irradiation; b) magnified STEM-EDS maps areas of conical shape structure profile and c) TEM, d) HRTEM and e) FFT HRTEM analysis of these areas

creases momentum along the normal to the sample surface. These bending strains lead to the formation of a parabolic shape structure. And with the power density rise the conical shape structure (parabolic systems with the additionally elongated central part) is formed. At such and lower power densities the film is heated to the values when stretching can be stopped by surface tension. The formation of a hole in the central part can be described by following dewetting processes in the melted part of the film with following increase of the power density.
The silicon thin layer provides additional impact to the hybrid system formation. The crystallization of silicon layer starts at the power densities lower that one needed for parabolic shape structure creation. In this case silicon crystallites starts to grow in the film volume but mixing with the gold layer does not take place. Such assumption is additionally supported by the presence of the second harmonic generation effect but the absence of white light signal (see figure 3). With the power density rise and formation of conical and hollow structures the volume of crystallites in the Si film start to grow as well as gold-silicon mutual mixing. As a result the white-light signal can be observed in photoluminescence spectra additionally to the second harmonic generation signal. In this case hydrodynamic interaction between silicon layer and silica substrate provides a momentum detaching central part of silicon film which is mostly crystallized. This effect can be seen on the HRTEM images of these structures in the central part.

2.2 Nonlinear optical properties studies

The observed internal composition of the parabolic, conical and hollow shape structures are in the direct connection with their non-linear optical properties. For the analysis of nonlinear optical properties of the structures we used the same femtosecond laser system with changed repetition rate to 80 MHz.

Collected optical signals from structures that were obtained under laser pumping with power 2 mJ/cm^2 are summarized in figure 3a.

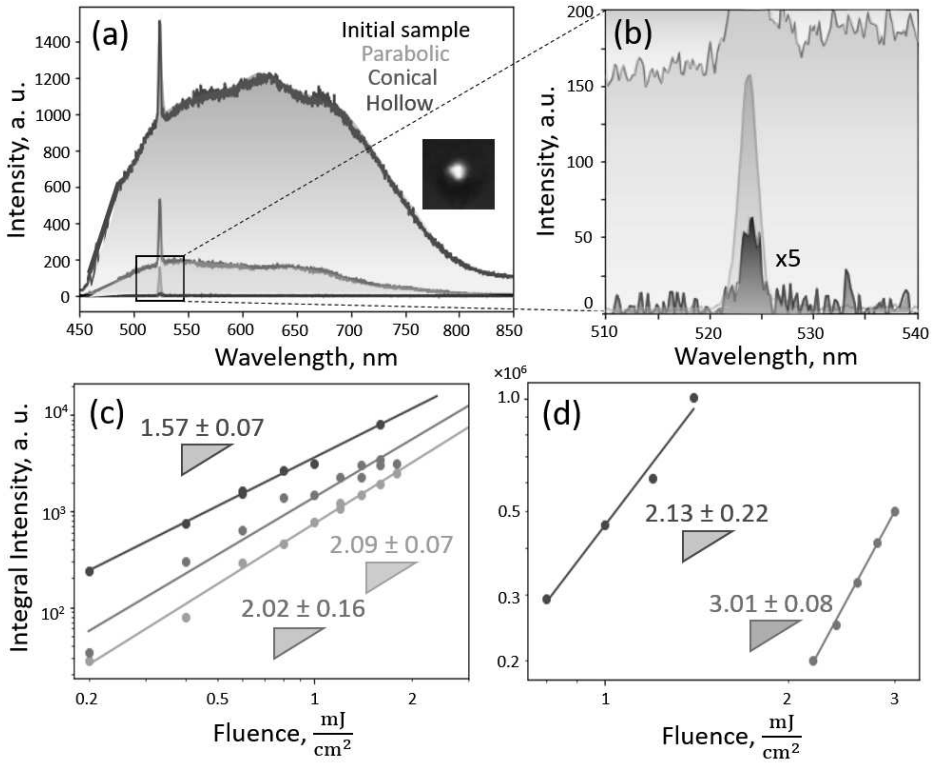

Figure 3: Nonlinear optical properties of hybrid structures; a) photoluminescence signal of initial film (black), parabolic (green), conical (blue) and hollow (red) structures;b) magnified area of the figure (a); Dependence of integral values of c) SHG and d) broadband photoluminescence signals on the pump power

A signal from initial sample (two-layered gold-silicon thin film) is demonstrated by a black curve on the plot. It can be seen that the non-radiated sample emits only a weak SHG signal at the wavelength of 525 nm under fs-laser pumping. The nature of this peak potentially is connected with a breaking of symmetry on surface defects [16]. The ten-times enhancement of SHG signal compared to the initial film was achieved from the parabolic shape structure (green curve). A possible mechanism of this enhancement is the local breaking of inversion symmetry [17] due to the creation of net of interfaces separating different crystalline silicon grains produced by laser radiation of sample. Even higher enhancement of the SHG signal was noticed from the conical shape structure (blue curve) which was twenty-times higher compared to the initial sample. However, in parallel with SHG signal, a broadband photoluminescence signal in almost whole visible range was observed. The same features of optical signal were noticed for hollow shape structure (red curve) but the intensity of signal was several times higher and it was seen even by a naked eye through micro-objective on the CCD camera as a white light point (see insert). The possible enhancement of white-light signal is connected with the open central part of the hollow shape structure. We suppose that this hole allows radiation to go outside the structure without absorption on the gold film. To understand the nature of these processes, nonlinear response measurements were performed. Figure 3b shows a nonlinear response for the SHG signal. The integral intensity of SHG was calculated by taking into account two edge points at 520 and 527 nm, which correspond to the transition between SHG and white light signals on the spectra. These points were reset to zero by baseline and integral values under obtained curves were calculated. These integral values corresponding to specific pump powers are marked by specific points in the plot (see Fig. 3c). A combination of these points for each structure type was approximated by lines and their slopes corresponded to the order of nonlinearity are shown. It can be seen that slopes for the SHG signal are close to 2 with errors ± 0.07 for parabolic and hollow

shape structures and ± 0.16 for conical shape structure. Thus the signals grow according to a quadratic law depending on pump power, which corresponds to the two-photon absorption process. The same dependencies were plotted for broadband photoluminescence signal. Integral intensities for this case were calculated by integration over the whole considered wavelengths range with subtraction of the integral value of the SHG signal. Results of these calculations are shown in figure 3d. The obtained slopes are 3.01 ± 0.08 for the conical shape structures and 2.13 ± 0.22 for the hollow ones. Based on these data it can be concluded that the two- and three-photon absorption processes make the main contribution to the white light photoluminescence signals. It is widely known, that efficiency of light absorption by silicon is low due to its indirect gap nature. The possible mechanism in our case leading to enhancement of absorption efficiency is hot carries injection from gold to silicon by two- and three-photon absorption processes [18]. We assume that further role plays a combination of radiative, Auger and defect assisted relaxation processes which lead to emission of photons with different energies and formation of broadband photoluminescence signal. These assumptions demonstrate a potential model of white light generation.
Thus, we have developed method of hybrid metal-dielectric structures fabrication with different non-linear responses from the same bi-layered Au-Si thin film. The control of the internal microstructure of the hybrid systems affecting on the non-linear response is controlled by simple variation of the laser beam parameters such as power density and number of incident pulses. It should be noted that even in the same type of hybrid structure (conical or hollow) the white-light luminescent spectra demonstrate inherent uniqueness caused by the morphology deviations of the structures geometry due to stochastic features of fabrication process as well as the surface inhomogeneity of the initial film. Such peculiarity in combination with the opportunities of easy changing of the structure type and their mutual spatial position open up good perspectives for the application of laser-fabricated hybrid stuctures for security labels.

2.3 Creation of security label patterns

The security labels are usually made of building blocks arranged on the surface on the specially selected patterns which is revealed under external stimuli, e.g. illumination on the determined wavelength in case of luminescent security labels. In our case due to flexibility of laser-assisted fabrication process the different types of hybrid nanosystems can be distributed over the film area on the selected pattern or in a random way. To demonstrate this opportunity we recorded two types of patterns (see figure 4a). The first one consist of randomly distributed in space parabolic and hollow structures. Second one represents a combination of conical and hollow structures ordered in recognisable image. Top images in figure 4a shows an optical image of these labels, the bottom ones demonstrate SEM microphotographs.
At the small optical magnification (no more than 10x) there are no clear differences observed among structures of the same type. However, using more precise equipment for visualization, such as an objective with high M and NA or SEM system, the slight difference for the hollow-shaped structures can be observed (see 4a). In this case the optical imaging was performed by an objective with parameters of M = 50x, NA = 0.42.
The non-linear optical response of the hybrid structures (relation of the intensities the SHG signal and WL luminescence) is directly connected with the structure type creating defined luminescent patterns. To demonstrate this, the nonlinear optical signal mapping of the structure patterns was done. The results of this mapping are illustrated in figure 4b. Top part of figure corresponds to the signal observed at the wavelength of 525 nm (SHG signal) while bottom one corresponds to the signal at the wavelength of 650 nm (the randomly selected wavelength from the broadband PL signal). From comparison between these figures it is clearly seen that for the maps at different wavelengths the non-linear signals from hollow shape structures is higher than for parabolic and conical structures. Additionally, the parabolic-shaped structures do not demonstrate WL signals and are therefore hidden on the luminescent map made at the wavelength of 650 nm. Thus, features of nonlinear signals of different types of structures can be used for creating protection levels authenticated under deep laboratory examination of the label.
In should be noted, that the shape of the white light photoluminescent signals for conical and hollow structures have deviations which are unique for each structure. This feature can be utilized for the cre-

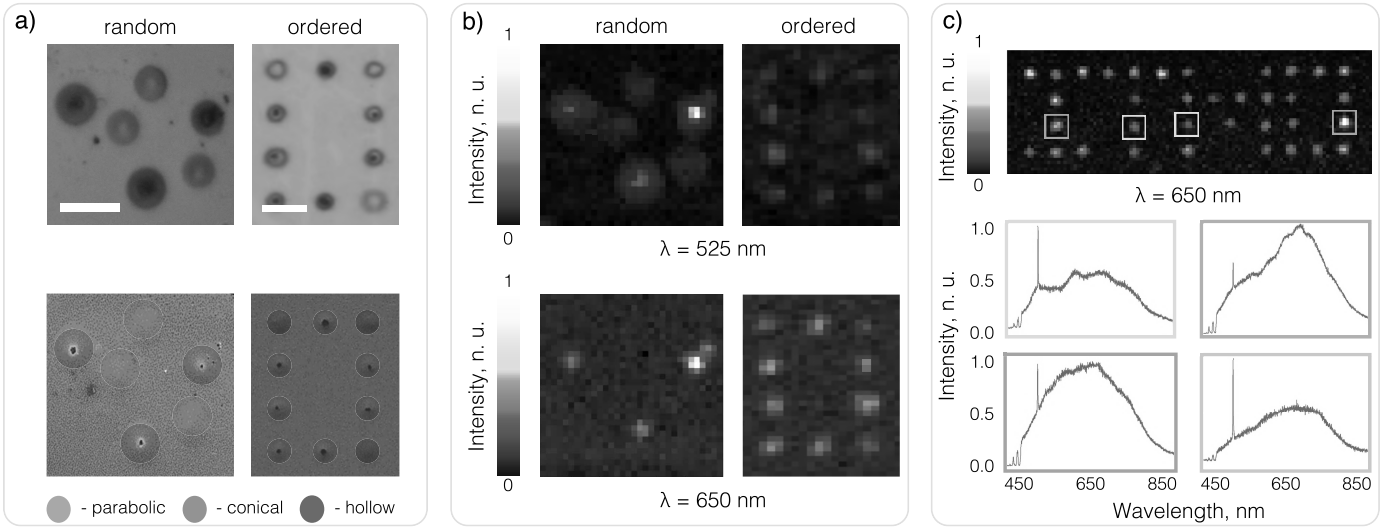

Figure 4: Femtosecond laser fabrication of gold-silicon structures for creation of unclonable security labels. a) Spatial location and combination of different types of structures; b) maps of the second harmonic generation signal (top) and white-light luminescent signal on the wavelength of 650 nm (bottom) for areas shown on (a); c) Demonstration of the PUF label recording. Scale bars correspond to 10 μm in figure (a) and XY μm in figure (c)

ation of the physically unclonable security labels. Such labels are based on features of stochastically distributed objects, e.g. luminescent signal[], Raman response[], etc. In our case the opportunity to fabricate hybrid structures on a predetermined pattern makes possible to create luminescent labels unifying benefits of conventional labels with determined distribution of its building elements and physically unclonable ones. Indeed, even in case of the space arrangement of the structures of the same type creating some picture or logo, the spectral shape of the white-light luminescent signals of its elements is stochastic.

For the demonstration of such design we have fabricated a logo consisted on the hollow-shaped structures demonstrating the WL signal with the intensity higher compared to other types of the structures (Fig. 4c). For the logo authentication some structures indicated by colorful boxes on the map are chosen. Then their nonlinear signals in the range from 450 to 650 nm are shown below the map in corresponding frames colors. The signal from one structure is consisted on some pixels, the amount of which is dependent on the scanning resolution. For the WL spectrum determination the signals from the pixels belonged to a certain structure are averaged and normalized to the signal maximum (see Supplementary materials, Section 2). Despite the fact that all considered structures look similar at the map, the shape and intensity of optical nonlinear signals for each structure are differ from each other. Thus, the fingerprints of the label elements include type of structure, its relative position, type of non-linear signal as well as white-light photoluminescence spectral signature. This information is digitized, stored and utilized during label identification on the scheme represented in Figure 5.

Firstly, a manufacturer choose a desirable security label configuration (type and mutual position of laser-induced structures) and produce it by previously discussed laser fabrication method. Further manufacturer records nonlinear signal map of the fabricated label. Then the non-linear spectra from each label element are averaged over the entire area of it, normalized and cleaned from the noise. Generally speaking, the non-linear PL spectra are quite close in terms of the SHG signal peak position and general spectral shape of the white-light signal. In fact, intensity/coordinate points describing the shape of the PL signal are correlated. So it is possible to recover the shape of the PL signal on the basis of some consistent point of the spectrum, which reduces the encoding capacity and can be used for the label hacking. In order to decorrelate points describing the obtained spectrum they are modified through a discrete cosine transform (see Supplementary materials, Section 3).

To find the key (Key 1) and helper data (HD), polar codes as component codes in the multilevel construction are applied to the transformed spectra (See Example 1 in Supplementary materials, Section

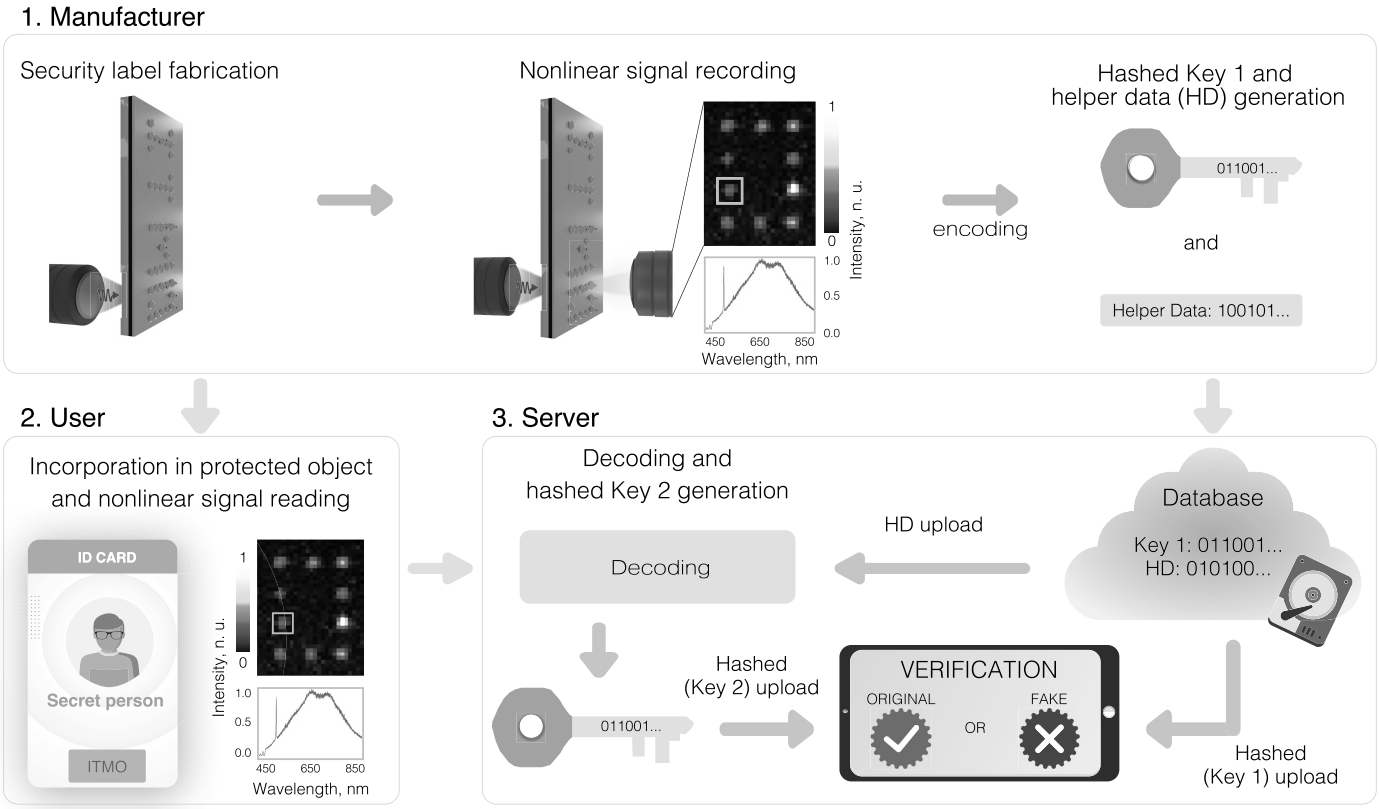

Figure 5: Potential scheme of object protection by the security label based on gold-silicon structures. Firstly, a manufacturer creates a security label and records its nonlinear signal map. The spectra averaged from each label elements are decorrelated via discrete cosine transform and converted to the Key 1 and Helper Data (HD) by polar codes. The obtained Key 1 is hashed and uploaded with HD to a database. At the next step, the user reads the label incorporated into a protective object. The obtained data and HD (requested from a database) are decoded. Then the Key 2 is generated, hashed and sent to verification. Finally, hashed Key 2 and Key 1 are compared.

3.). The obtained Key 1 is hashed and uploaded with HD to a database by manufacturer.
Further, a person, who wants to check the originality of the label (user), reads the label. Then the obtained data are decoded, and the Key 2 is generated utilizing HD. At the final stage hashed Key 2 and Key 1 are compared.
In case of coincidence of both hashed keys the label can be defined as original one. Results are sent to user with confirmation or rejection of the label originality. As a result, due to the uniqueness of each fabricated label, the user can be confident in the reliability of checked data results. Proposed scheme was applied to more than one hundred experimental spectra for identification of main parameters of the proposed PUF labels as the secret key length s, encoding capacity (EC) which equals to 2^s, bit uniformity and device uniqueness. Results of estimation are represented on table 1. The estimation details are represented in Supplementary materials, Section 3.

Table 1: PUF encoding parameters

Number of levels l	1				2				3				4			
n	128	256	512	1024	128	256	512	1024	128	256	512	1024	128	256	512	1024
Secret key length s	29	61	102	341	46	136	369	1114	47	153	457	1401	50	148	459	1452
Helper data size	99	195	410	683	210	375	654	933	307	577	1032	1614	333	675	1286	2201
Bit uniformity	0.54	0.50	0.49	0.50	0.53	0.50	0.50	0.50	0.53	0.50	0.50	0.50	0.52	0.50	0.49	0.50
Device uniqueness	0.91	0.99	0.99	0.99	0.94	0.99	0.99	0.99	0.94	0.99	0.99	0.99	0.99	0.99	0.99	0.99

As it is seen from the table, increase of number of levels in multilevel polar codes - l leads to nonlinear increase of secret key length s and for $l = 4$ it achieves 1452 which corresponds to EC for parabolic shape structure as 2^{1452} or $1.25{\times}10^{437}$. This value can be significantly increased taking into account an-

other protection features such as position and type of structure. For example, logo on figure 4c consists of 35 points of the same structure type. But each point can potentially represent one of three types of structures. Therefore, taking into account the structure type and their coordinates the encoding capacity of the demonstrated logo is 3^{35} or $5{\times}10^{16}$. This makes possible to use just the geometry features of the structures for additional level of the label protection. Therefore general EC of the logo can be estimated as $6.23{\times}10^{453}$ which fully satisfies the criterion for EC of physically unclonable labels exceeding the value of 10^{300} [19].
Another important parameter is bit uniformity which can be calculated by the formula (see Supplementary Information) and for ideal PUF label it should be close to 0.5. For our PUF labels this value is slightly varies around this value for $n \geq 256$, where n is amount of points in the spectrum. In case of luminescent labels based on white light luminescent building blocks, the device uniqueness is a crutial characteristic due to general similarity of the white-light luminescent spectra. In our case the device uniqueness is more than 0.9 for n equals to 128 and for $n \geq 256$ it corresponds to the value of 0.99. Therefore the application of the decorrelation procedure and polar codes provides high device uniqueness in the proposed PUF label design.

3 Conclusions

In summary, we have shown an approach for the non-linear optical response design in the metal-dielectric structures created by the direct fs-laser writing on the surface of bi-layered Au/Si thin films. We demonstrate a direct connection between their inner microstructure studied by HRTEM and non-linear optical signals (second harmonic generation and white light luminescence). The opportunity to control the type of the hybrid nanostructures by simple variation of power density and number of pulses as well as their spacial position opens up perspectives for the creation of luminescent security labels. We show that small deviations in the geometry of hollow-shaped structures modify inherent white light luminescent spectra. This feature is used for creation of the PUF labels based on white light luminescent elements. We demonstrate for the first time that in such labels the high degree of the device uniqueness (up to 99%) is supported by the decorrelation procedure and polar codes applied for the PL spectra of the structures. The obtained label characteristics allow to consider proposed design as a good platform for creation of security labels with physically unclonable elements, where uniqueness is supported by the unpredictable deviations of structures parameters from each other. Moreover our research provide new insights into the design of security labels based on white-light luminescence.

4 Experimental Section

Fabrication of initial sample:
Initially the bi-layered Au/Si films with thicknesses 30 and 90 nm correspondingly were fabricated on a silica substrate. The deposition of films was performed in two stages. Firstly, amorphous silicon layer was deposited on glass substrate by plasma-enhanced chemical vapor deposition from SiH4 precursor gas. Secondly, gold layer was deposited on top of silicon layer by magnetron sputtering.

Laser-assisted fabrication of hybrid structures :
Fabrication of structures was performed on the initial sample surface by a femtosecond laser system TEMA-150 (Avesta Project) with the wavelength of 1050 nm, pulse duration of 150 fs and repetition rate of 80 MHz. For better control of fabrication process, repetition rate was decreased to 1 Hz by passing through Pockels cell-based pulse picker (OG-V, Avesta project). Average output power varied from 5 to 20 mW depending on desirable resulting structure. The radiation with the following parameters was tightly focused on Au surface in a spot size with diameter of 4 µm from substrate side by Mitutoyo M Plan Apo NIR (M = x10, NA = 0.26) objective.
For recording arrays of structures, a piezo stage (AIST Project) was applied, which moves the sample in two perpendicular directions along the sample surface.

Outer geometry characterization:
For external geometry characterization of structures with high accuracy, both Scanning Electron Microscopy (SEM) and Atomic Force Microscopy (AFM) were used. SEM measurements were performed by Inspect (Field Electron and Ion Company, FEI) system in vacuum chamber under pressure 10^3-10^4 Pa and accelerating voltage 20 kV in mode of secondary electrons detection. AFM imaging was carried out by Ntagra Aura (NT-MDT) system in semi contact regime with passive vibration protection. Probes of HA NC series (NT-MDT) and W cathodes were used for scanning. Sample was scanned in ambient conditions.

Inner structure characterization:
Transmission electron microscopy (TEM) and scanning transmission electron microscopy (STEM) observations were performed with a microscope JEOL ARM200 cold FEG with 2 correctors. All STEM-EDX (Energy dispersive X-rays) maps were recorded using a JEOL Centurio detector (1sr). The cross-section TEM sample preparation is made by Focused Ion Beam (FIB) in a FEI Helio Nanolab 600i SEM (scanning electron microscope). A Pt layer is previously deposited on the surface of the sample to protect the surface during the cutting. All the structures were cut close to the middle of the shape.

Nonlinear optical signal measurements:
Photoluminescence (PL) and second harmonic generation (SHG) signals measurements were carried out under ultrafast laser pumping by the TEMA-150 fs laser with repetition rate of 80 MHz. Laser power was varied by attenuator in range of 5-50 mW for analyzing nonlinear properties and damage threshold of the structures. After going through attenuator, laser pulse was focused on the hybrid structures from the substrate side by objective by (M = 10x, NA = 0.26). Excited PL and SHG signals were collected by the VIS objective with M = 100x and NA = 0.70 from the top side of sample. Collected signal was sent to spectrometer Horiba Jobin-Yvon LabRam HR800 with diffraction grating 150 lines per mm while pumping signal was attenuated in 10^4 times by FESH850 filter which was placed before spectrometer.

Supporting Information
Supporting Information is available from the Wiley Online Library or from the author

Acknowledgements
Please insert your acknowledgements here

References

[1] W. Team, *https://www.who.int/multi-media/details/substandard-and-falsified-medicines-kill-hundreds-of-thousands-of-people-globally* .

[2] M. R. Carro-Temboury, R. Arppe, T. Vosch, T. J. Sørensen, *Science advances* **2018**, *4*, 1 e1701384.

[3] A. Abdollahi, H. Roghani-Mamaqani, B. Razavi, M. Salami-Kalajahi, *ACS nano* **2020**, *14*, 11 14417.

[4] Z. Zeng, B. Huang, X. Wang, L. Lu, Q. Lu, M. Sun, T. Wu, T. Ma, J. Xu, Y. Xu, et al., *Advanced Materials* **2020**, *32*, 43 2004506.

[5] X. Yu, H. Zhang, J. Yu, *Aggregate* **2021**, *2*, 1 20.

[6] V. P. Veiko, Y. Andreeva, L. Van Cuong, D. Lutoshina, D. Polyakov, D. Sinev, V. Mikhailovskii, Y. R. Kolobov, G. Odintsova, *Optica* **2021**, *8*, 5 577.

[7] S. Cucerca, P. Didyk, H.-P. Seidel, V. Babaei, *ACM Transactions on Graphics (TOG)* **2020**, *39*, 4 70.

[8] A. Y. Zhizhchenko, P. Tonkaev, D. Gets, A. Larin, D. Zuev, S. Starikov, E. V. Pustovalov, A. M. Zakharenko, S. A. Kulinich, S. Juodkazis, et al., *Small* **2020**, *16*, 19 2000410.

[9] S. Hayashi, K. Tsunemitsu, M. Terakawa, *Nano Letters* **2021**.

[10] A. O. Larin, L. N. Dvoretckaia, A. M. Mozharov, I. S. Mukhin, A. B. Cherepakhin, I. I. Shishkin, E. I. Ageev, D. A. Zuev, *Advanced Materials* **2021**, *33*, 16 2005886.

[11] Z. Ma, J. Zhou, J. Zhang, S. Zeng, H. Zhou, A. T. Smith, W. Wang, L. Sun, Z. Wang, *Materials Horizons* **2019**, *6*, 10 2003.

[12] S. Kalytchuk, Y. Wang, K. Polakova, R. Zboril, *ACS applied materials & interfaces* **2018**, *10*, 35 29902.

[13] J.-H. Wei, J.-F. Liao, L. Zhou, J.-B. Luo, X.-D. Wang, D.-B. Kuang, *Science Advances* **2021**, *7*, 34 eabg3989.

[14] Y. P. Meshcheryakov, N. Bulgakova, *Applied Physics A* **2006**, *82*, 2 363.

[15] A. Kuchmizhak, O. Vitrik, Y. Kulchin, D. Storozhenko, A. Mayor, A. Mirochnik, S. Makarov, V. Milichko, S. Kudryashov, V. Zhakhovsky, et al., *Nanoscale* **2016**, *8*, 24 12352.

[16] A. V. Zayats, T. Kalkbrenner, V. Sandoghdar, J. Mlynek, *Physical Review B* **2000**, *61*, 7 4545.

[17] S. V. Makarov, M. I. Petrov, U. Zywietz, V. Milichko, D. Zuev, N. Lopanitsyna, A. Kuksin, I. Mukhin, G. Zograf, E. Ubyivovk, et al., *Nano letters* **2017**, *17*, 5 3047.

[18] S. Makarov, I. S. Sinev, V. A. Milichko, F. Komissarenko, D. Zuev, E. V. Ushakova, I. Mukhin, Y. F. Yu, A. I. Kuznetsov, P. Belov, et al., *Nano letters* **2018**, *18*, 1 535.

[19] R. Arppe, T. J. Sørensen, *Nature Reviews Chemistry* **2017**, *1*, 4 1.